Materials Research Bulletin 76 (2016) 292–299

Contents lists available at ScienceDirect

Materials Research Bulletin

journal homepage: www.elsevier.com/locate/matresbu

Dielectric and ferroelectric properties modification of 0.7Pb$(Mg_{1/3}Nb2_{/3})O_3$–0.3Pb$(Zr_{0.52}Ti_{0.48})O_3$ ceramics by Ba$(Zn_{1/3}Nb_{2/3})O_3$

Hassakorn Wattanasarn[a], Wattana Photankham[a], Tosawat Seetawan[a,*], Rattikorn Yimnirun[b], Chanchana Thanachayanont[c], Napatporn Petnoi[d], Soodkhet Pojprapai[d]

[a] Center of Excellence on Alternative Energy, Program of Physics, Faculty of Science and Technology, and Research and Development Institute, Sakon Nakhon Rajabhat University 680, Nittayo Rd., Sakon Nakhon 47000, Thailand
[b] School of Physics, Institute of Science, and COE-NANOTEC-SUT on Advanced Functional Nanomaterials, Suranaree University of Technology, Nakhon Ratchasima 30000, Thailand
[c] National Metal and Materials Technology Center, National Science and Technology Development Agency, 114 Thailand Science Park, Phahonyothin Rd., Klong 1, Klong Luang, Pathumthani 12120, Thailand
[d] School of Ceramic Engineering, Institute of Engineering, Suranaree University of Technology, Nakhon Ratchasima 30000, Thailand

ARTICLE INFO

Article history:
Received 19 May 2015
Received in revised form 18 October 2015
Accepted 25 November 2015
Available online 10 December 2015

Keywords:
A. Ceramics
B. Phase transitions
B. Microstructure
D. Dielectric properties
D. Ferroelectricity

ABSTRACT

$(1-x)[0.7Pb(Mg_{1/3}Nb_{2/3})O_3$–$0.3Pb(Zr_{0.52}Ti_{0.48})O_3]$–$xBa(Zn_{1/3}Nb_{2/3})O_3$ of which $x = 0$, 0.025, 0.05, 0.075, and 0.1 ceramics were studied by a composite powder method and using a two-step sintering process. The morphology showed that the largest grain size was about 1.866 μm at $x = 0.1$, and the largest grain size of 3.81 μm at $x = 0.05$. The 0.7PMN–0.3PZT showed a decreased dielectric constant, posed dispersive phase transition and indicated relaxor ferroelectric when modified by BZN contents. The polarization from hysteresis loop measurements showed that saturated polarization, remnant polarization and coercive field decreased with increasing BZN. Increasing BZN not only exhibits electrostrictive behaviors with linear hysteresis loop shape but it is also a good candidate for lower power energy application. The largest strain of 0.122% was found at $x = 0.025$. These results clearly demonstrated the significance of the 0.7PMN–0.3PZT system activated by BZN.

1. Introduction

$Pb(Mg_{1/3}Nb_{2/3})O_3$ (PMN) ceramic is one of ferroelectric materials which exhibits linear electrostrictive and high dielectric properties [1–4]. At the same time, the $Pb(Zr_{0.52}Ti_{0.48})O_3$ (PZT) is well known among piezoelectric ceramics which have been investigated extensively [5,6]. The advantageous properties of normal ferroelectric PZT and relaxor ferroelectric PMN can be combined. The properties of $Pb(Mg_{1/3}Nb_{2/3})O_3$–$Pb(Zr_{0.52}Ti_{0.48})O_3$ (PMN–PZT) is expected to improve the piezoelectric and dielectric properties from the single system of either PZT or PMN [7–10]. Moreover, in the PMN–PZT ceramics, there is a presence of pyrochlore phase. Suppression of the pyrochlore phase can be achieved, not only by a sol–gel technique, but also two-step sintering with mixed oxide [11]. However, the dielectric constants of the mixed oxides form sol-gel are lower than a composite obtained from a solid state reaction. For the PMN–PZT system in which oxides were mixed together, previously, the researchers only focused on 0.7PMN–0.3PZT which is one of the materials at morphotropic phase boundary (MPB) [12,13]. The dielectric and ferroelectric properties at MPB composition of the PMN–PZT have been studied, but their temperature stability and reproducibility improvements are required due to fast reduction of the dielectric constant at lower and higher temperatures than at the maximum temperature. This introduces a narrow range for application, affecting various polarizations as a function of applied electric fields which are responded by frequencies as found in ferroelectric materials. Meanwhile, $Ba(Zn_{1/3}Nb_{2/3})O_3$; (BZN), one of the candidates for microwave dielectric materials, has been employed as resonators and filters for wireless communication technologies because the ordered structure in cubic perovskite results in high dielectric constant and low dielectric losses in the wavelength of micro and millimeter [14]. This suggests that BZN can be used for microelectronic wireless application.

The ceramic preparation process plays a crucial role in responses to the polar nanoregions. Therefore, this study expends the research on ceramics that are prepared with composite solid

* Corresponding author. Fax: +66 4 274 4319.
E-mail addresses: tseetawan@yahoo.com, t_seetawan@snru.ac.th (T. Seetawan).

http://dx.doi.org/10.1016/j.materresbull.2015.11.047
0025-5408/

state reaction of mixed oxides. The preparation of 0.7PMN–0.3PZT was obtained by columbite mixed oxide, while BZN composite was added into 0.7PMN–0.3PZT ceramics. In this study composed of analyzed microstructure and determined ferroelectric properties of $(1-x)[0.7Pb(Mg_{1/3}Nb_{2/3})O_3–0.3Pb(Zr_{0.52}Ti_{0.48})O_3]–xBa(Zn_{1/3}Nb_{2/3})O_3$; $(1-x)$[0.7PMN–0.3PZT]–xBZN where $x=0$, 0.025, 0.05, 0.075, and 0.1.

The microstructure, phase transition, crystal size, and theoretical density after sintering were studied. The ferroelectric property composing of dielectric constant, loss tangent, polarization, electric coercive field and strain loop characterization were investigated.

2. Experiment

The $(1-x)[0.7Pb(Mg_{1/3}Nb_{2/3})–0.3Pb(Zr_{0.52}Ti_{0.48})O_3]$–$x$BZN having $x=0$, 0.025, 0.05, 0.075, and 0.1, $(1-x)$(0.7PMN–0.3PZT)–xBZN were prepared by solid state reaction technique. The 0.7PMN–0.3PZT ceramics were prepared by columbite method. Barium zinc niobate [$Ba(Zn_{1/3}Nb_{2/3})O_3$; BZN] obtained with ZnO (99%), Nb_2O_5 and $BaCO_3$ (99%). $(1-x)$(0.7PMN– 0.3PZT)–xBZN were prepared from powers composed of reagent grade MN, PbO (99%) excess with 4 mol%, ZrO_2 (99%), TiO_2 (98%) and BZN. These powders were mixed and wet ball-milled for 24 h in deionize water, then vaporized by hotplate and heated to 850 °C for 4 h. The sample was crushed into powder and mixed with polyvinyl alcohol, and pressed into pellets at 190 MPa in disc shape with 20 mm and 1.8 mm for thickness. The samples were sintered at 1100 °C for 2 h, see the full synthesis details of PMN–PZT–BZN as previously reported [15].

Crystal structures of powder and sintered samples were studied using an X-ray diffractometer (Shimadzu XRD-6100). Diffraction intensity was measured in a range between 20° and 70° with a step-up of 0.02°. Density of the sample was measured by using Archimedes method. Microstructural characterization was carried out on the fractured surfaces of specimens using scanning electron microscopy (SEM). Grain sizes of sintered samples were estimated by a linear intercept method from SEM micrographs. Crystal sizes were estimated by transmission electron microscopy (TEM) using a JEOL JEM-2010 transmission electron microscope operated at an accelerating voltage of 200 kV. The samples were coated with silver paint on the sample surfaces as electrode for dielectric measurements. The capacitances were obtained using Chen Hwa 1061 LCR-Meter connected to the sample electrode surface. The samples were heated at temperature from 30 to 200 °C. In this study, the dielectric constants were measured at a discrete frequency range of 1–100 kHz. The ferroelectric hysteresis loops were characterized with high voltage from AC amplifier (Trek, model 20/20C) and the high voltage applied to the sample was connected with Sawyer–Tower circuit. The electric field was applied to the samples to induce strain behavior and was investigated by using a linear variable differential transducer (LVDT, Omron ZX-TDA11).

3. Results and discussion

3.1. Phase formation and microstructural characteristics

The XRD analysis of $(1-x)$[0.7PMN–0.3PZT]–xBZN ($x=0$, 0.025, 0.05, 0.075 and 0.1) ceramics, sintered at 1100 °C for 2 h, presents the characteristics of complex perovskite cubic $(A(B'B'')O_3)$. Fig. 1(a) shows that 0.7PMN–0.3PZT is an intermediate phase between tetragonal and cubic phase which is called the MPB composition [2,16]. With gradual addition of BZN content into 0.7PMN–0.3PZT, the 2θ peak slightly shifts to the right hand side and then shifts to the left hand. Table 1 shows lattice parameters a, c and relative density obtained from the XRD results from a 2θ range of 20–70°. Meanwhile, the c/a ratio reduces with increasing BZN content (see Table 1). This shows an effect of Ba^{2+} and Pb^{2+} substitution in A site, as well as Zn^{2+}/Nb^{5+} in B site of BZN. Agglomerates occur with Mg^{2+}/Nb^{5+} ions in PMN, whereas Zn^{2+}/Nb^{5+} ions are restricted only into Zr^{4+}/Ti^{4+} of PZT due to stability order [16,17]. In order to determine phase transition of various samples accurately, the broad peaks of (2 0 0) plane lines of five samples obtained by extraction from XRD pattern range 44–45° as presented in Fig. 1 (inset). The (2 0 0) reflections is on the XRD study. Gaussian peaks (red and green lines) were fitted with two curves on the (2 0 0) reflections split to (0 0 2) and (2 0 0) tetragonal phase which are in tetragonal phase of 0.7PMN–0.3PZT. It is noted

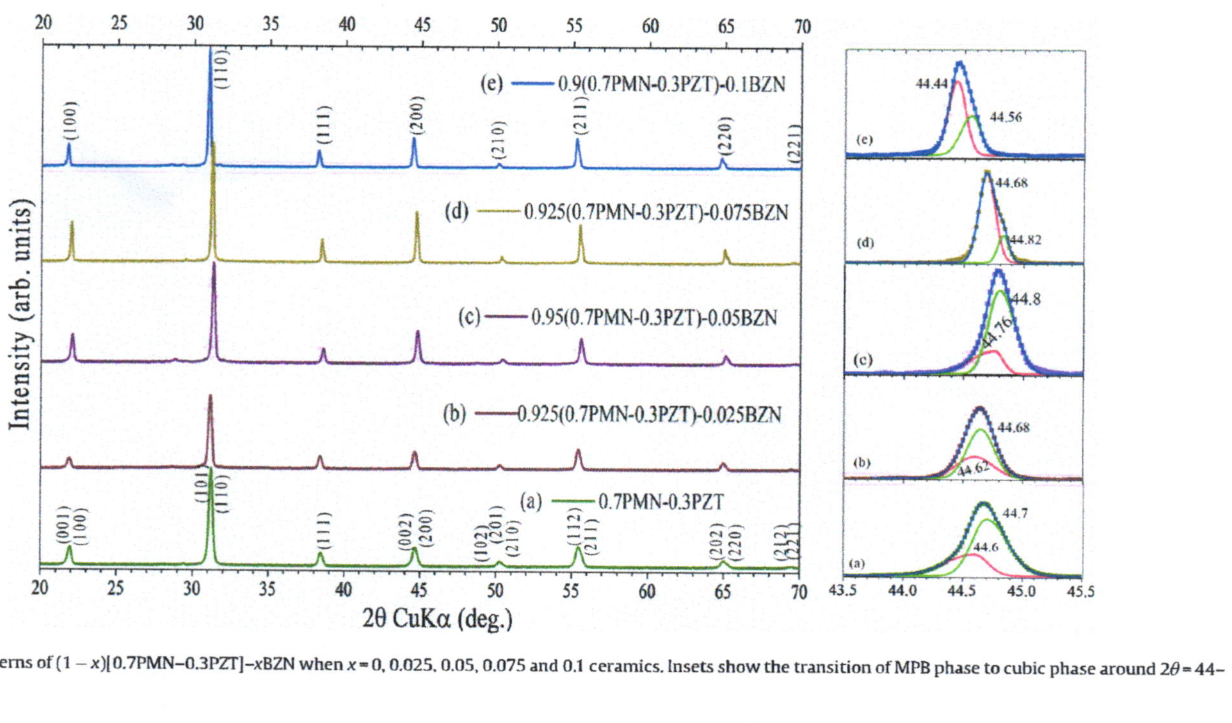

Fig. 1. XRD patterns of $(1-x)$[0.7PMN–0.3PZT]–xBZN when $x=0$, 0.025, 0.05, 0.075 and 0.1 ceramics. Insets show the transition of MPB phase to cubic phase around $2\theta=44–45°$.

Table 1
Lattice parameters a and c, tetragonality (c/a), Rietveld refinement using data from 20 to 70° of the XRD results in Fig. 1. Crystallite sizes obtained from TEM, density, and relative density (TD) of $(1-x)$(0.7PMN–0.3PZT)–xBZN ceramics when $x=0$, 0.025, 0.05, 0.075, and 0.1.

BZN contents	a (Å)	c (Å)	c/a	Crystal size (μm)	Average grain size (μm)	Density (g/cm^3)	TD (%)
$x=0$	0.4036	0.4067	1.0077	0.527	1.54, 3.58[a], 1.45[b]	7.71, 7.78[a], 6.78[b]	94.53, 96.13[a], 83.77[b]
$x=0.025$	0.4045	0.4068	1.0057	0.923	3.48	7.66	94.51
$x=0.05$	0.4043	0.4065	1.0055	1.293	3.81	7.64	94.83
$x=0.075$	0.4038	0.4060	1.0054	1.369	2.68	7.64	95.06
$x=0.1$	0.4046	0.4066	1.0049	1.866	2.09	7.62	95.52

[a] Sol–gel method.
[b] Solid state reaction process [11].

that the samples peaks shifted. With gradually increasing BZN content, the integrated intensity of (2 0 0) tetragonal phase decreases, while the intensity of (2 0 0) tetragonal phase shifted to (2 0 0) cubic phase, as shown in Fig. 1 (inset), because the Zn^{2+}/Nb^{5+} ions can agglomerate with the Mg^{2+}/Nb^{5+} ions easier than Zr^{4+}/Ti^{4+}. It should be noted that for $x=0.025$ sample, the pseudo-cubic structure was also clearly detected as shown in Fig. 1 (b). This observation indicated that only a small amount of the Zn^{2+}/Nb^{5+} ions initially substitute into 0.7PMN–0.3PZT structure. Additionally, for the MPB, it is well known that there is coexistence between region of the tetragonal and cubic phases of equal quantities [18,19]. Consequently, BZN originated form agglomerates of Ba^{2+} and Zn^{2+}/Nb^{5+} ions into 0.7PMN–0.3PZT structure in mixed oxide composite was possible, it transforms to cubic perovskite with increasing BZN content.

In order to determine the agglomerates of particles after sintering of $(1-x)$[0.7PMN– 0.3PZT]–xBZN, Fig. 2 reveals that the mixed oxides with composite powders consisting of incorporated nanoparticle. The polygon crystal shapes of 0.7PMN–0.3PZT are shown in Fig. 2(a). The BZN particles are mixed with the 0.7PMN–0.3PZT. The 0.7PMN–0.3PZT crystal transforms to a rectangular shape with increased BZN content. Moreover, stacking faults are observed in the samples suggesting that the increased atomic species make difficult for the constituent atoms into the ordered structure [20]. An average crystallite size increases with increasing BZN content, see Table 1, an increase in sintering temperature is responsible for the increased crystallite size.

The SEM fractured surface micrographs of $(1-x)$[0.7PMN–0.3PZT]–xBZN samples are shown in Fig. 3. The morphology of 0.7PMN–0.3PZT fractured surface as shown in Fig. 3(a) clearly shows that PMN consists of fine grain, and the agglomerates are untightened. In contrast, PZT powder consists of agglomerates with larger polygon grain [11]. The grain growth is shown in Fig. 3(c), due to the liquid phase of PbO rich that rapidly volatilized, which led to the development of densification of samples. Besides, inhomogeneous microstructure and coarse grain variation were observed in the micrograph [21]. Fig. 3 exhibits micrographs of $(1-x)$[0.7PMN–0.3PZT]–xBZN. The average grain size initially increases from 1.54 μm for $x=0$–3.81 μm for $x=0.05$, then decreases to 2.09 μm for $x=0.1$ as listed in Table 1. Generally, it is a good idea to observe the microstructure of porous ceramics with data on grain size and grain boundary which is determined from physical models by using measurements based on bulk density. Further addition the theoretical density increases with increasing BZN content, see Table 1. The grain size is affected by the sintering temperature for BZN that is known to be higher than 0.7PMN–0.3PZT [22]. This suggests that the two-step sintering is an easy preparation route for $(1-x)$(0.7PMN–0.3PZT)–xBZN ceramics which is a mixed powder method that the advantages are a bigger quantity per batch and a lower cost than sol–gel method. The solid state reaction (SR) using the two-step sintering method is a technique to avoid lead vacancy from PMN and PZT. Also, the sol–gel method is more time consuming and more chemical quantity required for synthesis. In addition, it is difficult to control the carbon dioxide content in the sol–gel method. In a typical solid state reaction, two-step sintering can control the carbon dioxide of $BaCO_3$ for synthesizing the BZN powder. In this study, the average grain size, density, and relative density of $(1-x)$(0.7PMN–0.3PZT)–xBZN prepared by the two-step sintering, sol–gel and solid state reaction process are compared and listed in Table 1. These results show that the average grain size, density, and relative density obtained from two-step sintering are lower than those from sol–gel process but higher than solid state reaction process.

3.2. Dielectric properties

The two-step sintering process of 0.7PMN–0.3PZT exhibits the dielectric properties at room temperature, the dielectric constant maximum, and the temperature of dielectric maximum lying between those prepared by sol–gel and by solid state reaction process. The dielectric properties at room temperature, the

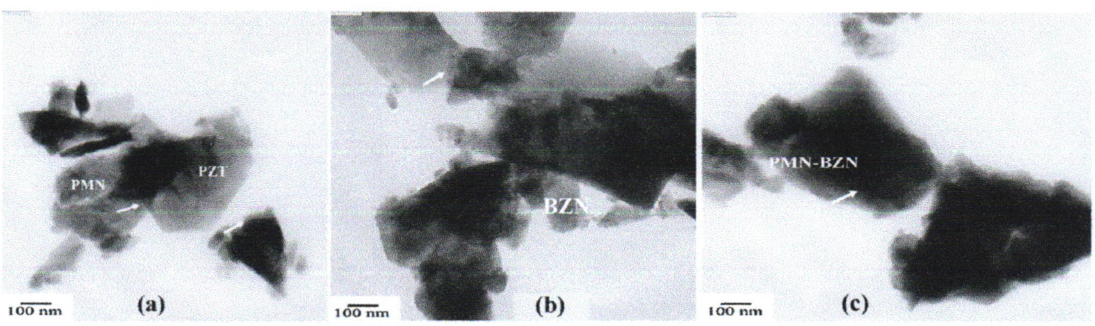

Fig. 2. TEM micrographs of $(1-x)$[0.7PMN–0.3PZT]–xBZN ceramics with stacking faults (see arrow), synthesized from the mixed oxide, $x=$(a) 0, (b) 0.05, and (c) 0.1.

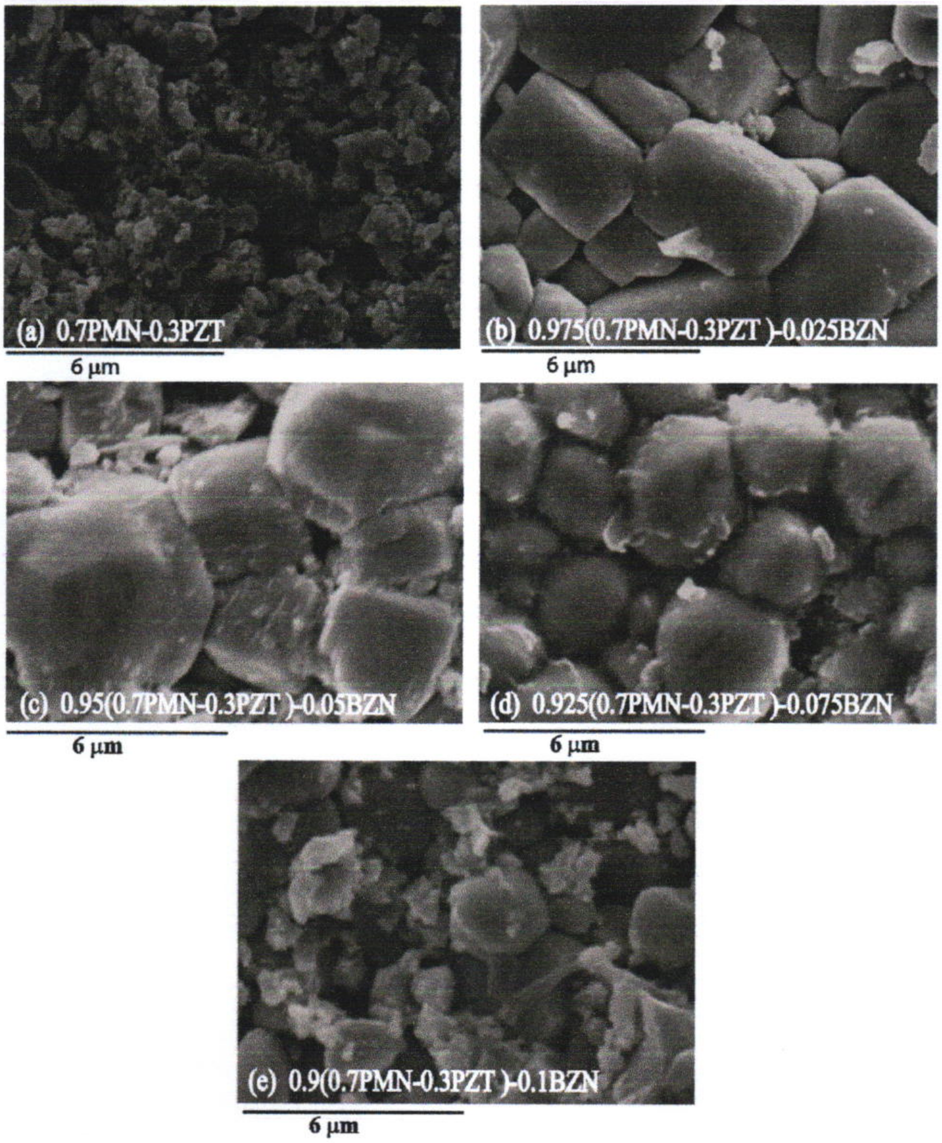

Fig. 3. SEM micrographs from fractured surface of $(1-x)$(0.7PMN–0.3PZT)–xBZN ceramics sintered at 1100 °C while x is equal to (a) 0, (b) 0.025, (c) 0.05, (d) 0.075 and (e) 0.1.

dielectric constant maximum, and the temperature of dielectric maximum $(1-x)$(0.7PMN–0.3PZT)–xBZN ceramics samples are also higher than sol–gel process but lower than SR process as listed in Table 2. The dielectric properties (ε_r) of 0.7PMN–0.3PZT is a function of temperature that shows phase transition at temperature 116 °C and then rapidly decreases as shown in Fig. 4(a). It is noted that the phase transition of 0.7PMN–0.3PZT in the two-step sintering process occurs at a transition temperature higher than the sol gel process [11] and the SR process [10]. Moreover, 0.7PMN–0.3PZT is a normal ferroelectric material where PMN exhibits relaxor ferroelectric behaviors as a result of a short range ordered structure with heterogeneity in the mixed oxide powder. When BZN, which is a microwave dielectric material, is added to 0.7PMN–0.3PZT, the dielectric constant is observed to significantly

Table 2
Dielectric properties of $(1-x)$(0.7PMN–0.3PZT)–xBZN ceramics when x = 0, 0.025, 0.05, 0.075, and 0.1 (at 1 kHz) at room temperature (RT), dielectric dispersion maximum (δ), dielectric constant maximum, and temperature of dielectric maximum (T_{max}).

x	Dielectric properties (RT)				δ (°C)	Dielectric properties at T_{max}				T_{max} (°C)	
	ε_r		tanδ			ε_r		tanδ			
0	1322		0.043		112	5598		0.033		116	
0.025	1349		0.054		90.6	3077		0.044		96	
0.05	3621		0.067		80.5	5024		0.065		82	
0.075	3159		0.041		70	3508		0.024		30	
0.1	3598		0.026		20	3598		0.026		29	
0.7PMN–0.3PZT	SG. 1219	SR. 5600	SG. 0.015	SR. 0.057		SG. 1321	SR. 10100	SG. 0.035	SR. 0.057	SG. 0.035	SR. 0.057

SG. is mixed oxide by sol gel process [11], SR. is composite by solid state reaction [10].

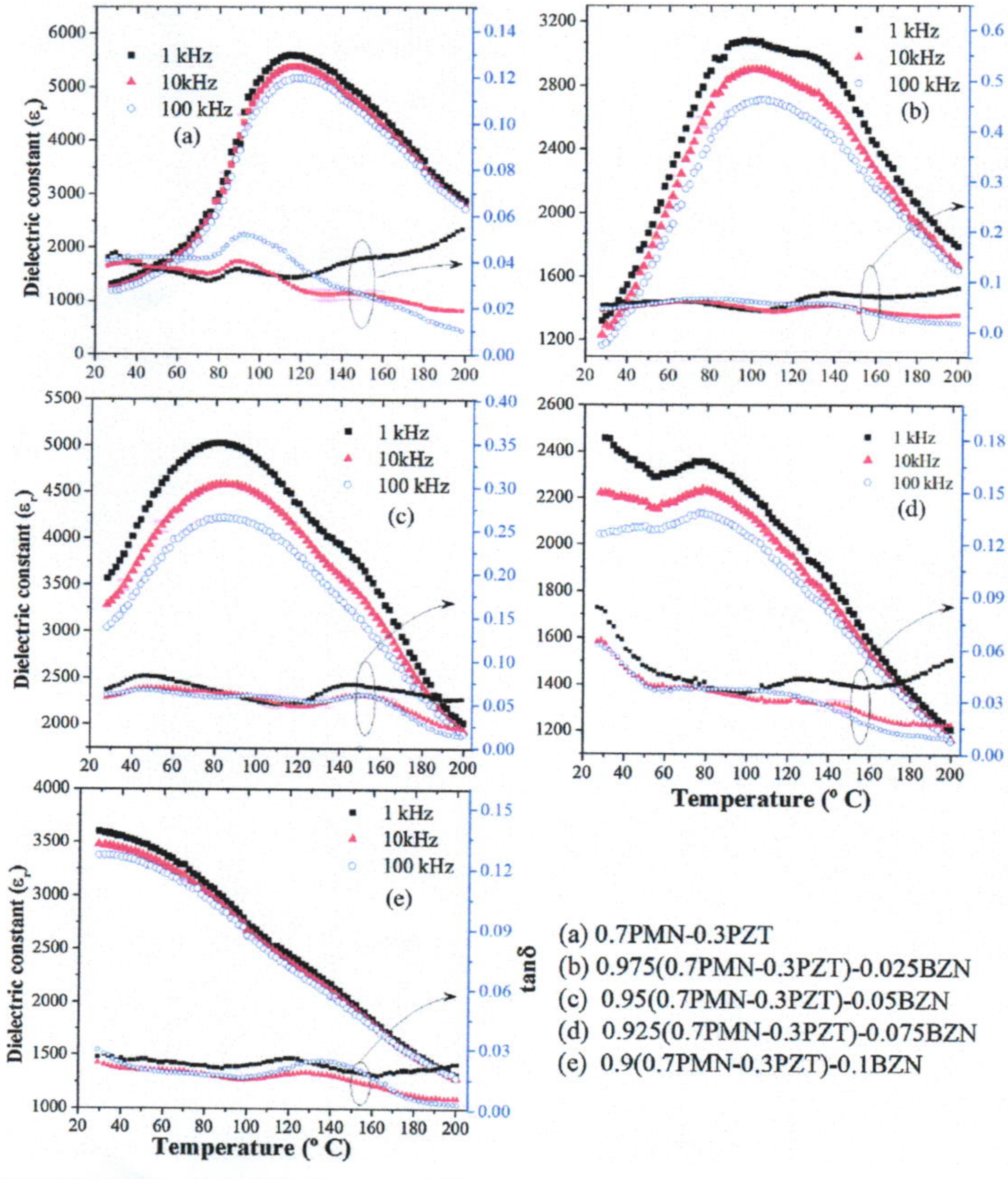

Fig. 4. Temperature and frequency dependence of dielectric constant and dielectric losses of $(1-x)$(0.7PMN–0.3PZT)–xBZN ceramics; (a) $x=0$, (b) $x=0.025$, (c) $x=0.05$, (d) $x=0.075$, and (e) $x=0.1$.

decrease with increasing BZN content as listed in Table 2. While adding BZN contents of 0.025, 0.05 and 0.075 into 0.7PMN–0.3PZT, Fig. 4(b–d) show dielectric constants as a function of temperature response for dipolar system, board peaks of dielectric dispersion and phase transitions in agreement to the previous explanation [15]. It is noted that the microwave dielectric materials are sensitive to temperature and frequency. In Fig. 4(b), when $x=0.025$, a peak at 96 °C is observed. The BZN with $x=0.05$ shows a peak at 80 °C as shown in Fig. 4(c), with a peak shift to lower temperature when the frequency increases. Similarly, BZN with $x=0.075$ depicted in Fig. 4(d), at high frequency, shows two peaks at 30 °C and 70 °C, with a lower dielectric constant at higher frequency. This suggests that both temperature and high frequency sensitively affect to the phase transition of 0.7PMN–0.3PZT when gradually added with BZN. For $x=0.1$, a peak of dielectric constant has been diffused phase transition at lower than 30 °C and followed by the rapidly decreased values with increasing temperature. This indicates a relaxor ferroelectric behavior. For $x=0.025$, 0.05, and 0.075, dielectric constant patterns were alike, having been frequency dispersion of samples as presented in Fig. 4(b–d). The broad peak of dielectric dispersion and phase transition show relaxor behavior [2,23].

The dielectric properties of adding BZN into 0.7PMN–0.3PZT are listed in Table 2. The highest of dielectric constants of $(1-x)$(0.7PMN–0.3PZT)–xBZN when $x=0.05$ at temperature 30 °C. The maximum value of the dielectric constant decreases with increasing frequency at room temperature, as well as decreased with slightly increasing BZN content. On the other hand, it was observed that the grain size increases with decreasing dielectric constant at temperature of dielectric maximum. It suggests that the dielectric properties of two-step sintered 0.7PMN–0.3PZT are comparable to those prepared by sol–gel and solid state reaction technique. The dielectric constants of the two-step sintered 0.7PMN–0.3PZT are higher than sol–gel method but lower than solid state reaction method [10,11].

Fig. 5(a–e) show loss tangent (tanδ) dependence with frequencies of

$(1-x)$(0.7PMN–0.3PZT)–xBZN at different temperatures. It is found that the tanδ values are high at higher temperatures and the tanδ decreases with increasing frequency of the applied alternative current. This may be due to the hopping of electrons that cannot follow the frequencies of applied current. It is noted that the dispersion of tanδ at higher temperatures is observed. This is attributed to the conductivity of the ceramics, resulted from the oxygen vacancies, and PbO evaporated during higher temperature sintering.

A relaxor behavior is observed from dielectric constant curve. The effect of BZN on the dispersion slope of the dielectric constant curve was investigated. The dielectric peak in high a temperature range was fitted to the Lorentz-type empirical relation that introduced by Bokov and Ye for discuss the dielectric constant of relaxor ferroelectric behavior as follow [24],

$$\frac{\varepsilon_A}{\varepsilon} = 1 + \frac{(T - T_A)^2}{2\delta^2}$$

where $T_A(< T_m)$ and $\varepsilon_A(> \varepsilon_m)$ are the fitting parameter for the temperature and the maximum value of the dielectric constant (magnitude of the Lorentz peak), respectively, δ is as a measure of the degree of dielectric dispersion maximum, T (T_m) and ε (ε_m) are the temperature at dielectric constant maximum of the sample, respectively. The δ value of $(1-x)$(0.7PMN–0.3PZT)–xBZN are given in Table 2. It found that δ value at 112° for x = 0, and decreases with the increasing BZN content, meanwhile, the lowest of δ was anticipated at 19° for x = 0.1, corresponds with dielectric constants as shown in Fig. 4. The T_m decreases together with showing relaxor behavior when BZN content is increased. The dielectric dispersion maximum of 0.7PMN–0.3PZT has been strongly affected by BZN content. Consequently, adding BZN into PMN induces increases in size and interaction strength of polar clusters in polar nano-domains [25].

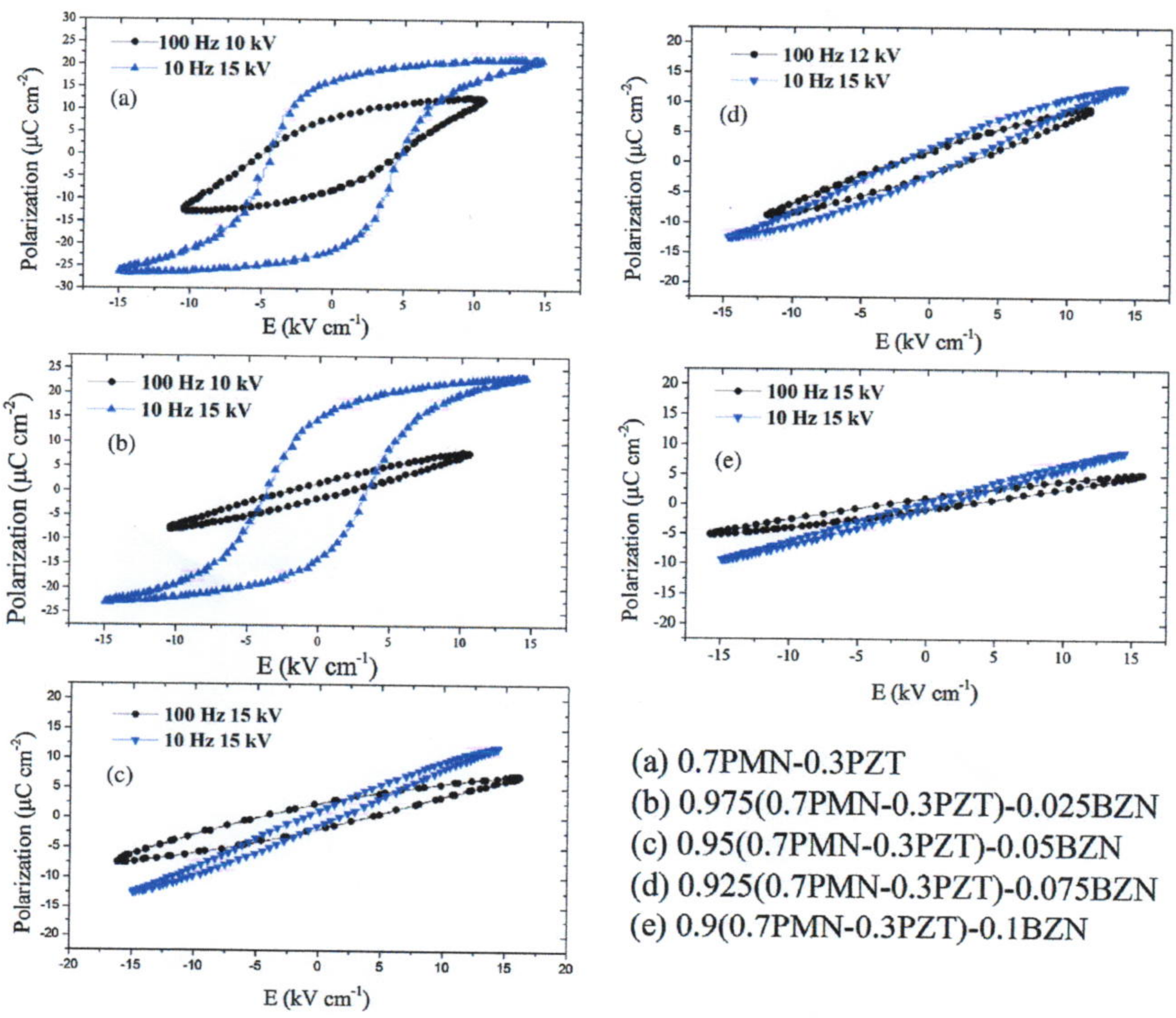

Fig. 5. Polarization hysteresis loops of $(1-x)$(0.7PMN–0.3PZT)–xBZN at x = 0, 0.025, 0.05, 0.075, and 0.1 ceramics.

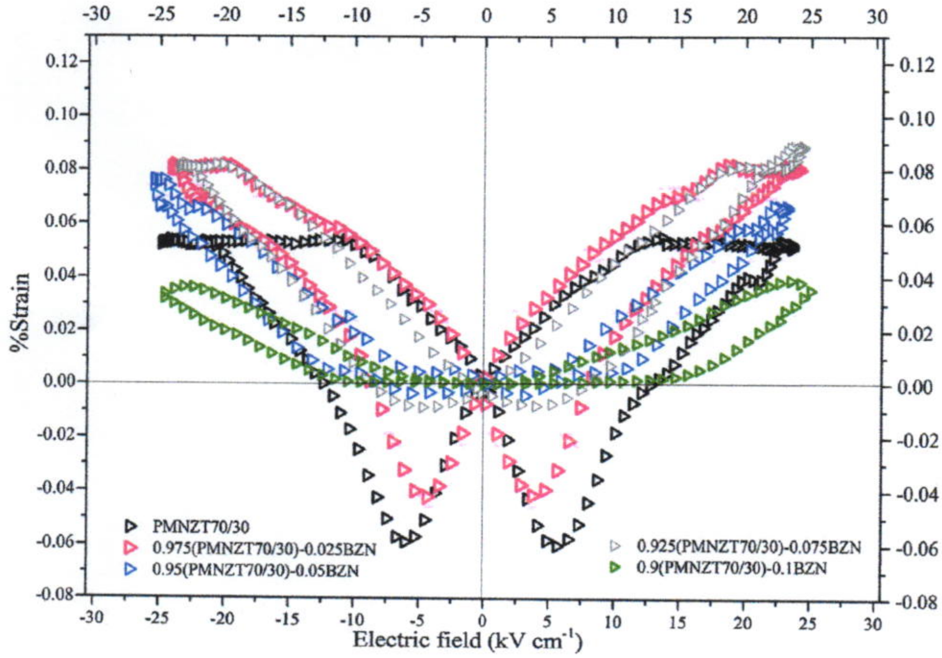

Fig. 6. Strain loops for compositions with different BZN content measured at room temperature.

3.3. Electric field induced polarization hysteresis loops

Fig. 6 illustrates the investigated polarization from hysteresis loops which can be used to indicate domain switching of the 0.7PMN–0.3PZT doped with BZN ceramics. The hysteresis loop shape varies greatly with the ferroelectric ceramic composition at room temperature. Polarization hysteresis loops for 0.7PMN–0.3PZT ceramic, as shown in Fig. 5. It is noted that MPB phase as a result of the 0.7PMN–0.3PZT in the slim hysteresis loops at 10 Hz, having smaller difference between saturated polarization (P_s) and remnant polarization (P_r). Coercive field (E_c) has a low value of which the ferroelectric micro-domain state containing a long range order that is a characteristics of the suppressed dipole–dipole interaction. This is a characteristic of a ferroelectric behavior [10]. In the case of the BZN added into the 0.7PMN–0.3PZT, the squareness hysteresis loop becomes slim flat with increasing the BZN content, as illustrated in Fig. 5(b–d), at an applied electric field of 15 kV cm^{-1} at 10 Hz. The domain switching applied by electric field is studied. It suggests that the sample is poled by applied electric field. A charge is injected through microstructure of pseudo-cubic perovskite and then domain switching. Increasing amount of Zn^{2+}/Nb^{5+} ions agglomerated with Mg^{2+}/Nb^{5+} ions rapidly decreases P_s and P_r at $x = 0.025$. The P_s and P_r of $x = 0.05$ and $x = 0.075$ are constant, and then decreases at $x = 0.1$. Besides, polarization hysteresis loop of $(1-x)$(0.7PMN–0.3PZT)–xBZN of which an applied electric field was applied at a frequency of 100 Hz were investigated, as illustrated in Fig. 5. By adding BZN into 0.7PMN–0.3PZ, it is found that hysteresis loops were pinched, of which P_s was lower than at 10 Hz, regarding to the largest electric field (before electrical breakdown) applied to the samples for the samples with various BZN contents, due to the different electrical resistivity, compositional heterogeneity and porosity of the samples [15], as seen from the relative density when BZN was added into 0.7PMN–0.3PZT (Table 1). It should then be noted that in this experiment the constant applied electric field of 10–15 kV cm^{-1} was applied to all samples due to the limitation explained above. Moreover, the domains rapidly reverse due to an ease in micro-domain movement, when the electric field is applied into the microstructure of cubic phase with more highly ordered structure. In contrast, it is believed that hopping mechanism of surplus Zn^{2+} ion in this stoichiometric is possible and it will give a higher probability for a hop across the lower barrier.

3.4. Electric field induced strain loop characterization

To investigate a characteristic of $(1-x)$(0.7PMN–0.3PZT)–xBZN ceramics for actuator applications, the bipolar strain of samples that demonstrates strain loop shape under applied electric field 25 kV cm^{-1} at room temperature and at 50 mHz are shown in Fig. 6. With further BZN addition, strain values compared to the pure 0.7PMN–0.3PZT show that the sample having $x = 0.025$ has a large strain of 0.122%, while the negative strain reduces from 0.06% for $x = 0$ to 0.01% for $x = 0.1$. This implies that the dominant ferroelectric behavior in 0.7PMN–0.3PZT is disturbed by BZN addition. Usually, domain wall exists in the MPB phase or nonpolar phase that can transform to normal ferroelectric by an applied electric field [26]. However, when BZN content was increased to $x = 0.1$, the pseudo-cubic pronounced nonpolar phase, affecting the transformation of ferroelectric to nonpolar resulting in reduction of strain values.

4. Conclusions

$(1-x)$[0.7PMN–0.3PZT]–xBZN, having $x = 0$, 0.025, 0.05, 0.075 and 0.1, ceramics were prepared from BZN addition into 0.7PMN–0.3PZT. Using the two-step sintering process is a choice for tuning both microstructure and electrical properties of which are between sol–gel process and solid state reaction process. X-ray diffraction technique showed peak shifts indicating phase transitions. After a gradually increase of BZN contents, the structures of the ceramics experienced a gradual transition from MPB phase to cubic phase. Crystallite sizes are in a range of 0.527–1.866 μm. The largest $(1-x)$[0.7PMN–0.3PZT]–xBZN grain size of 3.81 μm was obtained for $x = 0.05$ and then decreased with increasing BZN content. The dielectric constant measurement taking place over temperature of 30 °C is in a range of 1300–3600 at a frequency of 1 kHz. The results indicated that the dielectric properties of the 0.7PMN–0.3PZT followed that of relaxor ferroelectric when $x = 0.025$, 0.05, and 0.1. The degree of diffuseness decreases slightly when BZN is added to 0.7PMN–0.3PZT. The temperature of dielectric maximum was obtain at composition at 1 kHz of $x = 0$ ($\varepsilon_r = 5600$). The dielectric dispersion maximum of 0.7PMN–0.3PZT has been strongly affected by BZN content, i.e. the highest is 112° for $x = 0$, and decreased with increasing BZN content. From the hysteresis loops, it is found that for the PMN–PZT–BZN system, not only the relaxor ferroelectric behavior gradually decreased to soft relaxor but also MPB phase transition gradually shifted to cubic phase with increasing BZN content. The saturated polarization, remnant polarization and coercive field values decreased with increasing BZN because of increased pseudo-cubic and relaxor ferroelectric content. While increasing BZN not only exhibited electrostrictive behaviors with linear hysteresis loop shape but it was also a good candidate for lower power energy application. The strain loop induced by an applied electric field at 25 kV cm $^{-1}$, the largest of strain of 0.122% was obtained at $x = 0.025$. These results exhibited the effects of microwave dielectric material on ferroelectric material behavior. This may be useful in capacitor applications.

References

[1] V. Koval, C. Alemany, J. Briancın, H. Brunckova, K. Saksl, J. Eur. Ceram. Soc. 23 (2003) 1157–1166.
[2] A.J. Moulson, J.M. Herbert, Electroceramics, Materials, Properties, Applications, 2nd ed., John Wiley & Sons Ltd., 2003.
[3] S. Jiansirisomboon, K. Songsiri, A. Watcharapasorn, T. Tunkasiri, Curr. Appl. Phys. 6 (2006) 299–302.
[4] R. Tipakontitikul, S. Ananta, R. Yimnirun, Curr. Appl. Phys. 6 (2006) 307–311.
[5] H. Ouchi, K. Nagano, S. Hayakawa, J. Am. Ceram. Soc. 48 (1965) 630–635.
[6] H. Ouchi, J. Am. Ceram. Soc. 51 (1968) 169–176.
[7] R. Yimnirun, S. Ananta, E. Meechoowas, S. Wongsaenmai, J. Phys. D: Appl. Phys. 36 (2003) 1615–1619.
[8] T.R. Shrout, A. Halliyal, Am. Ceram. Soc. Bull 66 (4) (1987) 704–711.
[9] A. Halliyal, U. Kumar, R.E. Newnham, L.E. Cross, Am. Ceram. Soc. Bull. 66 (1987) 671–676.
[10] R. Yimniruna, S. Ananta, P. Laoratanakul, J. Eur. Ceram. Soc. 25 (2005) 3235–3242.
[11] P. Moetakef, Z.A. Nematib, J. Alloy Compd. 476 (2009) 791–796.
[12] M. Sebastian, Dielectric Materials for Wireless Communication, 1st ed., Elsevier, 2008.
[13] S.F. Wang, Y.R. Wang, C.Y. Liu, W.S. Hsieh, Ceram. Int. 38 (2012) 1127–1132.
[14] H. Hughes, D.M. Iddles, I.M. Reaney, Appl. Phys. Lett. 79 (2001) 2952–2954.
[15] H. Wattanasarn, W. Photankham, T. Seetawan, R. Yimnirun, C. Thanachayanont, Ceram. Int. 41 (2015) 8367–8376.
[16] Z. Xia, Q. Li, Acta Mater. 55 (2007) 6176–6181.
[17] C. Thanachayanont, V. Yordsri, S. Kijamnajsuk, N. Binhayeeniyi, N. Muensit, Mater. Lett. 82 (2012) 205–207.
[18] Z. Xia, Q. Li, Solid State Commun. 142 (2007) 323–328.
[19] S.M. Gupta, D. Viehland, J. Appl. Phys. 83 (1998) 407–414.
[20] L.L. Hsiung, M.J. Fluss, S.J. Tumey, B.W. Choi, Y. Serruys, F. Willaime, A. Kimura, Phys. Rev. B 82 (2010) 184103.
[21] J.P. Guha, J. Mater. Sci. 34 (1999) 4985–4994.
[22] D.G. Morris, M.A. Morris, Acta Metall. Mater. 39 (1991) 1763–1770.
[23] D.K. Das-Gupta, P.C.N. Scarpa, IEEE Elect. Insul. Mag. 15 (1999) 23–32.
[24] A.A. Bokov, Z.G. Ye, J. Mater. Sci. 41 (2006) 31–52.
[25] M. Promsawat, A. Watcharapasorn, H.N. Tailor, S. Jiansirisomboon, Z.G. Ye, J. Appl. Phys. 113 (2013) 204101.
[26] A. Ullah, C.W. Ahn, I.W. Kim, Curr. Appl. Phys. 10 (2010) 1367.

Journal Search

Search query

in Journal Title ▼ Search

☐ Exact phrase

Materials Research Bulletin

Country: United Kingdom

Subject Area: Engineering | Materials Science | Physics and Astronomy

Subject Category:

Category	Quartile (Q1 means highest values and Q4 lowest values)															
	1999	2000	2001	2002	2003	2004	2005	2006	2007	2008	2009	2010	2011	2012	2013	2014
Condensed Matter Physics	Q2	Q2	Q2	Q2	Q2	Q2	Q2	Q2	Q2	Q2	Q2	Q2	Q2	Q2	Q2	Q2
Materials Science (miscellaneous)	Q2	Q2	Q2	Q2	Q1	Q2	Q2	Q2	Q2	Q2	Q1	Q1	Q1	Q2	Q2	Q2
Mechanical Engineering	Q2	Q2	Q2	Q2	Q1	Q1	Q2	Q1	Q1	Q1	Q1	Q1	Q1	Q1	Q2	Q1
Mechanics of Materials	Q2	Q2	Q2	Q2	Q2	Q2	Q2	Q2	Q2	Q2	Q2	Q1	Q1	Q2	Q2	Q2

Publisher: Elsevier Limited. **Publication type:** Journals. **ISSN:** 00255408

Coverage: 1966-2015

H Index: 75

Scope:

Materials Research Bulletin is an international rapid publication journal reporting research on the synthesis, processing, structure and properties of inorganic [...]
Show full scope

Charts Data

SJR indicator vs. Cites per Doc (2y)

The SJR indicator measures the scientific influence of the average article in a journal, it expresses how central to the global scientific discussion an average article of the journal is. Cites per Doc. (2y) measures the scientific impact of an average article published in the journal, it is computed using the same formula that journal impact factor ™ (Thomson Reuters).

Citation vs. Self-Citation